Thermo-Calc Determination of Phase Diagram and Thermodynamic Properties of Ni-Al Binary System

Ben Festus * and Peter Apata Olubambi

Posted Date: 21 June 2023

doi: 10.20944/preprints202306.1488.v1

Keywords: Phase stability; Gibbs energy; Ni-Al alloy; Thermodynamic properties; Phase diagram; Thermo-Calc; Calphad; Activities

Article

Thermo-Calc Determination of Phase Diagram and Thermodynamic Properties of Ni-Al Binary System

Ben Festus [a,b]* and Peter Apata Olubambi [b]

[a] Department of Physics, Federal Polytechnic Ede, Ede, Nigeria
[b] Centre for Nanoengineering and Tribocorrosion (CNT), University of Johannesburg, Johannesburg, South Africa
* Correspondence: Tel: (+234) 7030067492; E-mail: festusb@uj.ac.za, benfestus@federalpolyede.ed.ng

Abstract Ni-Al alloys have good corrosion-resistant properties making them preferable as a material of choice compared to ordinary metals. A good understanding of the phase diagram and thermodynamic properties of the Ni-Al alloy binary system is essential in determining relevant industrial applications of the system. The Ni-Al phase diagram is being reassessed since those found in the literatures are based on very old experimental studies. The phase diagram and thermodynamic properties of the Ni-Al alloy is determined using the Thermo-Calc 2022b software over a temperature range of 200 K to 2000 K and 1 atm of pressure. A total of nineteen fields (including elemental Al and Ni) comprising of five single solid phases, one liquid phase, and twelve double regions was obtained from the equilibrium calculation. The thermodynamic calculation has six invariant reactions comprising of two eutectic reactions (914.83 ± 0.025 K and 1641.80 ± 0.025 K), three peritectic reactions (1123.55 ± 0.025 K, 1400.72 ± 0.025 K and 1642.65 ± 0.025 K), and one peritectoid reaction (913.96 ± 0.025 K). The solubility of Al in Ni is also determined. The Thermo-Calc temperature – composition of the Ni-Al alloy is compared with the existing experimental studies to identify the physical properties of the different thermodynamic properties of the Ni-Al alloy binary system.

Keywords: Phase stability; Gibbs energy; Ni-Al alloy; Thermodynamic properties; Phase diagram; Thermo-Calc; Calphad; Activities

1. Introduction

Phase diagrams have been identified as one of the fundamental building blocks of an alloy system from which system stability can be deduced as a function of composition and temperature [1–3]. Experimental measurements of some systems using phase equilibrium and thermodynamic properties are sometimes relatively expensive and time-consuming [4]. Using well established thermodynamic models embedded in the Thermo-Calc software makes the process relatively easier and cheaper [5,6].

Ni forms a cubic crystal and has a silvery-white appearance. As a transition metal, Ni is hard and ferromagnetic with good strength and corrosion resistance properties. This unique properties is no doubt one of the reasons why Ni-based alloys is widely used in making coins, wires, batteries, magnets, amongst others [7–9]. Al on the other hand like Ni is silvery-white and has excellent corrosion resistance. Al however is a light weight metal malleable and easy to cast and machine [10–12]. Well known alloy of Ni includes Cr, Fe, Mo and Cu, this is because these alloys have high temperature scaling with exceptional strength and good resistance to corrosion properties. The Ni-Al alloy have equally been found to possess good mechanical properties with a high degree of resistant to corrosion. The Ni-Al alloy is equally characterized by high-temperature strength, low density and brittleness at high and room temperatures [13]. The Ni-Al alloy has been utilized in nickel-base superalloys to increase the resistance of the superalloy at high temperatures to oxidation and sulfidation [14,15].

Preprints (www.preprints.org) | NOT PEER-REVIEWED | Posted: 21 June 2023 doi:10.20944/preprints202306.1488.v1

The Ni-Al alloy binary system has been analysed in different studies with researchers adopting different experimental techniques [15–19]. These studies are however old and has lots of discrepancies in the reported results. One of such discrepancies is the controversies surrounding the invariant reaction temperatures at the Ni-rich side of the alloy where four different studies [20–24] supported the results obtained by Hansen and Anderko [19] while others [15,16] supported the result obtained by Schramm [18] with the result of the latter deviating as much as 33 K and 25 K from that of the former for the two invariant reactions investigated. Interestingly, the results reported by Hansen and Anderko had become an adopted literature standard for the invariant reactions occurring at the Ni-rich side [15].

Understanding the thermodynamic properties of the Ni-Al alloy (also regarded as a superalloy) is important in applications such as gas turbines, metal welding and cutting, emergency flares and beacons, and as a demolition device [25]. CALPHAD method has been used to assess the thermodynamic properties of different alloys including the Ni-Al alloy binary system [26–28]. However, like the phase diagrams, these results are old and needs to be reassessed. This study thus seeks to address some of the observable pitfalls by using a well robust and efficient database simulation software like the Thermo-Calc to re-assess the phase diagram and thermodynamic properties such as Gibbs energy, molar enthalpy and activity curve of the Ni-Al alloy with a view to better understand the thermodynamic nature of the alloy for more advanced industrial applications.

2. Methodology

Thermo-Calc software uses the CALPHAD method to calculate thermodynamic properties of a material system in order to understand properties such as solubility limits, phase diagrams, phase formation phase transition, temperature transformation, phase compositions and amounts, amongst others [1,16,17]. The CALPHAD uses established experimental data represented as polynomials of chemical composition and temperature to derive thermodynamic functions of a material system and subsequently stores same in a database [30]. The database is then used to provide a function of temperature and composition for different material properties [2]. Numerical optimization techniques makes it easy to obtain the values of the polynomial coefficients [3,31]. For thermodynamic calculations, the Thermo-Calc software uses a state that minimizes the total Gibbs free energy to generate internally consistent thermodynamic datasets [5].

In this study, the equilibrium phase diagram of the Ni-Al alloy binary system was calculated using the Thermo-Calc 2022b software. As in previous works [32–36], the binary calculation template was used to calculate the equilibrium phase diagram for the Ni-Al alloy phase diagram over a temperature range from 200 K to 2000 K at a total pressure of 1 atm. The thermodynamic properties such as activity curves, enthalpy and Gibbs energy was subsequently determined using the type "Gibbs energy curves" over different temperature range. For all calculations, the TCBIN: TC Binary Solutions v1.1 database was used to obtain all the plots for the Ni-Al alloy binary system.

3. Results and Discussions

3.1. Phase Diagram Properties

Figure 1 displays the plot of the temperature-composition phase diagram calculation of the Ni-Al alloy binary system with the composition represented by mass percent. This phase diagram is in agreement with that obtained by Refs. [26,37,38]. From the figure, a total of nineteen phase fields including elemental Al and Ni was obtained from the equilibrium phase calculation. Three single solid phases namely BCC_B2, D513_Al_3Ni_2, and FCC_L12#2 other than liquid phase, elemental Al (FCC_Al), and elemental Ni (FCC_Ni) at the terminals was obtained from the equilibrium phase calculation. Aside the phase diagram, Figure 1 shows that the orthorhombic DO11_Al_3Ni, and Al_3Ni_5 phases can be considered as line compounds. The three solid phases identified in Figure 1 are also referred to as the intermetallic phase with the cubic BCC_B2 phase denoted as AlNi, the cubic FCC_L12#2 phase denoted by $AlNi_3$, and the hexagonal D513_Al_3Ni_2 phase denoted as Al_3Ni_2. The

Preprints (www.preprints.org) | NOT PEER-REVIEWED | Posted: 21 June 2023 doi:10.20944/preprints202306.1488.v1

cubic BCC AlNi and FCC $AlNi_3$ are the most explored and practically important compound of the Ni-Al alloy for development of Ni-based superalloys for high temperature materials [13–15,38,39].

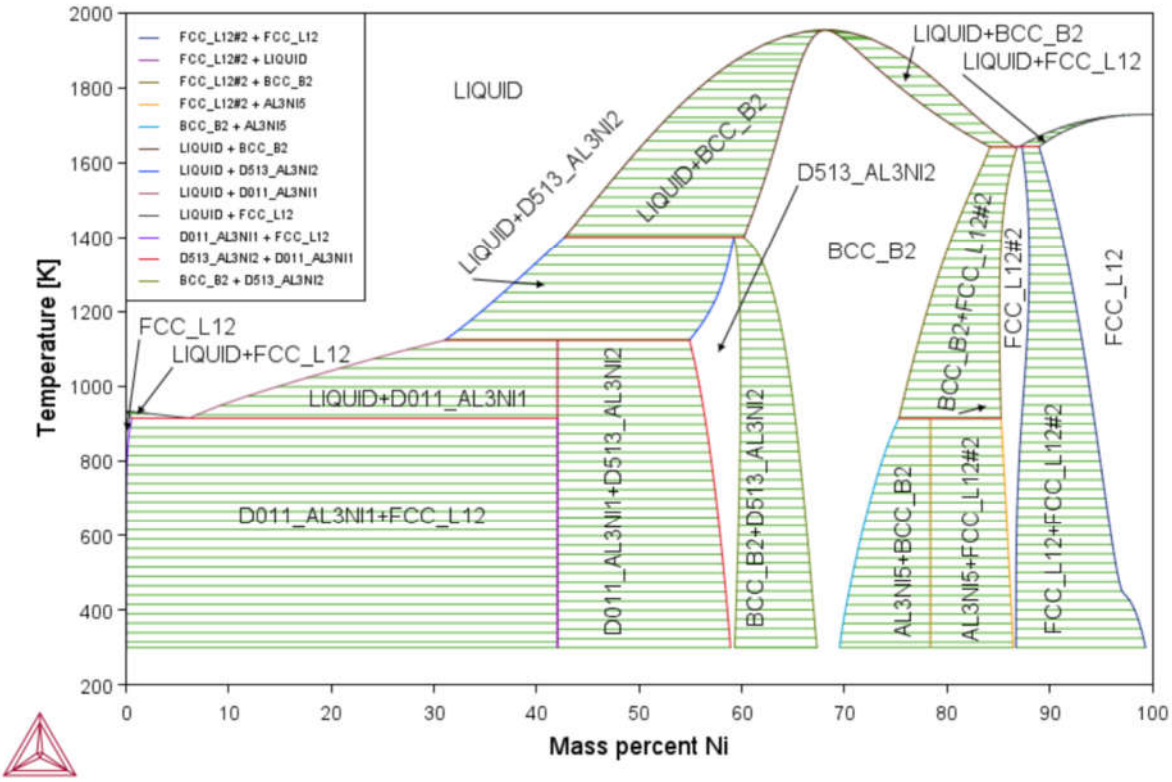

Figure 1. Phase diagram of the Ni-Al alloy binary system obtained in this study.

From Figure 1, a total of thirteen fields of two mixed phases is obtained namely LIQUID + FCC_Al at a Ni mass percent of 0-6.15 and temperature range of 914.83 K - 933.47 K, LIQUID + D011_ Al_3Ni at a 6.15-42.03 Ni mass percent and 914.83 K – 1123.55 K temperature range, LIQUID + D513_Al_3Ni_2 at Ni mass percent of 31.07-59.20 and temperature range of 1123.55 K to 1400.72 K, LIQUID + BCC_B2 at a 42.72-86.56 Ni mass percent and 1400.72 K to 1952.96 K, LIQUID + FCC_L12#2 extending from 86.56-87.03 Ni mass percent and 1641.80 K to 1642.65 K temperature range, LIQUID + FCC_Ni extending a temperature range of 1642.65 K to 1728.25 K at a 87.03-100 Ni mass percent, D011_ Al_3Ni + FCC_Al at a Ni mass percent of 0-42.03 and temperature range of 300 K to 914.83 K, D011_ Al_3Ni + D513_Al_3Ni_2 at a Ni mass percent of 42.03-58.89 and temperature range of 300 K to 1123.55 K, BCC_B2 + D513_Al_3Ni_2 at a 59.20-67.31 Ni mass percent and 300 K to 1400.72 K temperature range, Al_3Ni_5 + BCC_B2 at a 69.52-78.38 Ni mass percent and 300 K to 913.96 K temperature range, Al_3Ni_5 + FCC_L12#2 at a 78.38-86.43 Ni mass percent and 300 K to 913.96 K temperature range, BCC_B2 + FCC_L12#2 at a 75.29-86.82 Ni mass percent and 913.96 to 1641.80 temperature range, and FCC_Ni + FCC_L12#2 at a Ni mass percent of 86.71-99.34 across a temperature range of 300 K to 1642.65 K.

Six invariant reactions are obtained from the equilibrium phase diagram of the Ni-Al alloy binary system as seen in Figure 1. The invariant reactions formed include two eutectic regions, three peritectic regions and one peritectoid region. Figures 2 to 4 are enlarged portions of Figure 1 used to investigate these invariant reactions. Figures 2a shows the first eutectic reaction (equation 1) of the Ni-Al alloy binary system occurring at eutectic temperature of 914.83 K (641.84 ^{0}C) and composition ratio of 6.15 Ni mass percent while the second eutectic reaction (equation 2) as seen in Figure 2b occurs at a temperature of 1641.80 K (1368.65 ^{0}C) and eutectic composition ratio of 86.56 Ni mass percent. The eutectic reaction observed at the Al-rich side of the Al-Ni which results in the formation of the cubic BCC Al_3Ni superstructure phase is consistent with the literature value of 640 ^{0}C reported by [13] and differs by 14 K when compared with the result obtained by [38]. The eutectic reaction at

Preprints (www.preprints.org) | NOT PEER-REVIEWED | Posted: 21 June 2023 doi:10.20944/preprints202306.1488.v1

the Ni-rich side has been a subject of controversies for decades with two different phase diagrams reported for this region. This study however differs slightly from the experimental result obtained by Refs. [20,21,23,24,38,40] but agrees with the experimental values reported by Refs. [15,18,41]. The reasons for the conflict in phase diagram at the Ni-rich side can be attributed to the quality of Ni and Al samples used and the wrong melting point value selected for Ni [15,41].

$$Liquid \leftrightarrow FCC\_Al + D011\_Al_3Ni \quad (1)$$

$$Liquid \leftrightarrow BCC\_B2 + FCC\_L12\#2 \quad (2)$$

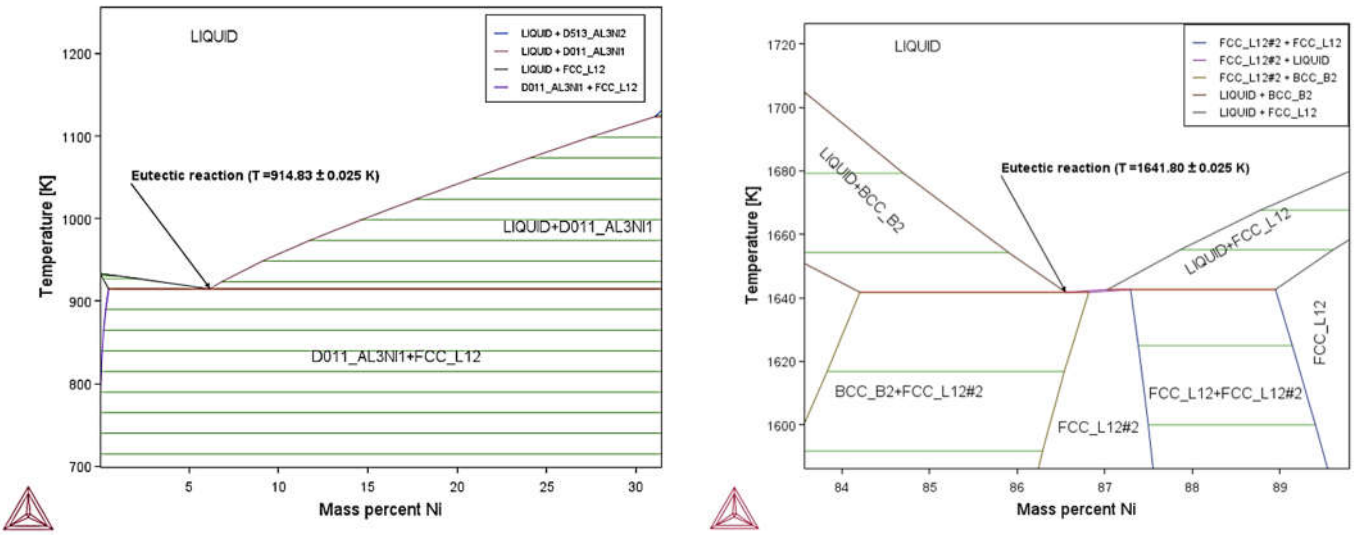

(a) (b)

Figure 2. Enlarged portions of Figure 1 showing eutectic reactions of the Al-Ag alloy binary system at (a) Al-rich side and (b) Ni-rich side.

Figures 3a to 3c shows the three different peritectic invariant reactions formed by the Ni-Al alloy binary system. Figure 3a shows the formation of a non-congruently melting cubic BCC Al_3Ni compound at the first peritectic region (equation 3) occurring at 42.03 Ni mass percent and temperature of 1123.55 K. This result is consistent with the experimental values obtained by Refs. [22,25,26]. Figure 3b also shows the formation of a second peritectic region (equation 4) for a hexagonal Al_3Ni_2 intermediate phase predicted at a temperature of 1400.72 K and 59.20 Ni mass percent composition. These values are consistent with the experimental values of 1405 K and 1406 K recorded by Refs. [25] and [22] respectively. However, it differs from the experimental result of Ibrahin et. al at 1410.30 K [26], and Pasturel et. al at a higher value of 27 K and 56 K peritectic melting temperature obtained for the cubic Al_3Ni and hexagonal Al_3Ni_2 compounds respectively [38]. The third peritectic region (equation 5) as seen in Figure 3c occurs at 1642.65 K peritectic temperature and composition of 87.30 Ni mass percent for the FCC_$AlNi_3$. This peritectic decomposition of the FCC $AlNi_3$ superstructure occurring at the Ni-rich side of the alloy has also been a subject of controversy with claims that it is sensitive to values of the three phases energies, responsible for determination of the equilibrium properties [38]. The peritectic temperature of $AlNi_3$ assessed in this study is consistent with the experimental results reported by [15,16,25,26,42], but about 7 K lower to the values recorded by [16,18], and 15-25 K higher than the experimental values reported by [19–24]. The purity of the metal samples used could be responsible for this huge variation observed in the peritectic temperature of $AlNi_3$ phase.

$$Liquid + D513\_Al_3Ni_2 \leftrightarrow D011\_Al_3Ni \quad (3)$$

Preprints (www.preprints.org) | NOT PEER-REVIEWED | Posted: 21 June 2023 doi:10.20944/preprints202306.1488.v1

$$Liquid + BCC\_B2 \leftrightarrow D513\_Al_3Ni_2 \quad (4)$$

$$Liquid + FCC\_AlNi \leftrightarrow FCC\_L12\#2 \quad (5)$$

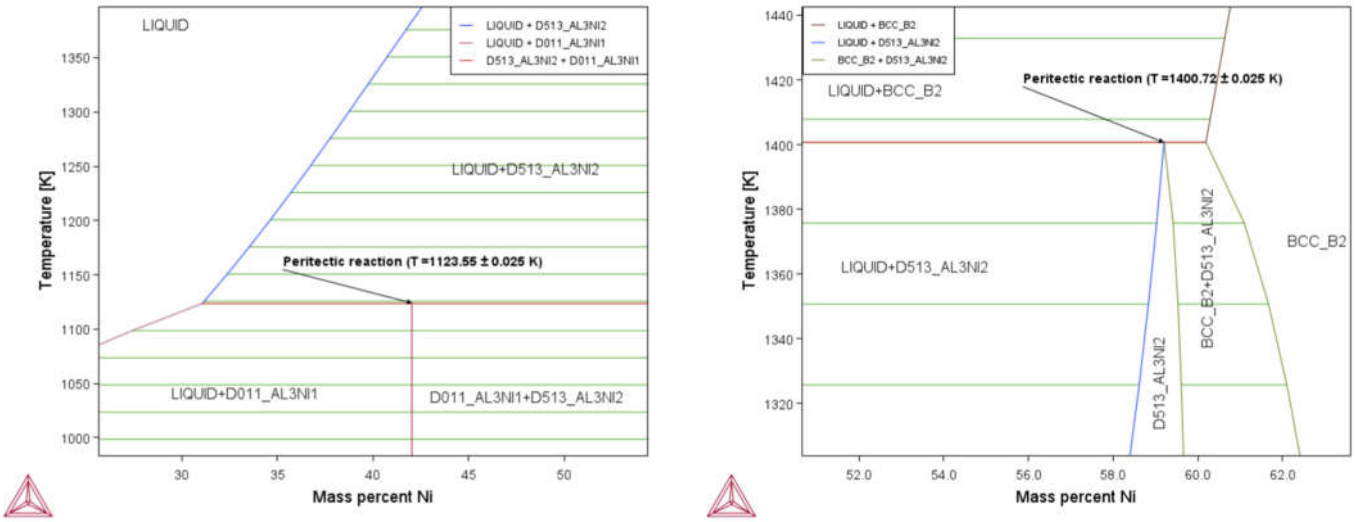

(a) (b)

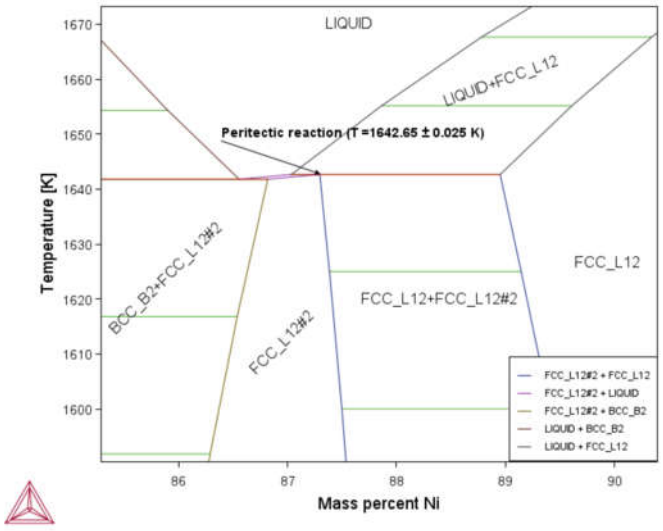

(c)

Figure 3. Enlarged portions of Figure 1 showing the (a) peritectic reaction for Al_3Ni (b) peritectic reaction for Al_3Ni_2 and (c) peritectic reaction for FCC_L12#2.

Figure 4 shows the peritectoid region (equation 6) obtained from the phase diagram calculation of the Ni-Al alloy binary system with the formation of Al_3Ni_5 phase observed to occur at 78.38 Ni mass percent and a temperature of 913.96 K. This result of the peritectoid temperature obtained in this study differs largely from the reported value of 973 K [26,43] despite a consistent Ni mass percent composition values for the phases involved i.e. 85.26, 75.29, and 78.38 for FCC_L12#2 ($AlNi_3$), BCC_B2 (AlNi), and Al_3Ni_5 phases respectively.

$$BCC\_B2 + FCC\_L12\#2 \leftrightarrow Al_3Ni_5 \quad (6)$$

Preprints (www.preprints.org) | NOT PEER-REVIEWED | Posted: 21 June 2023 doi:10.20944/preprints202306.1488.v1

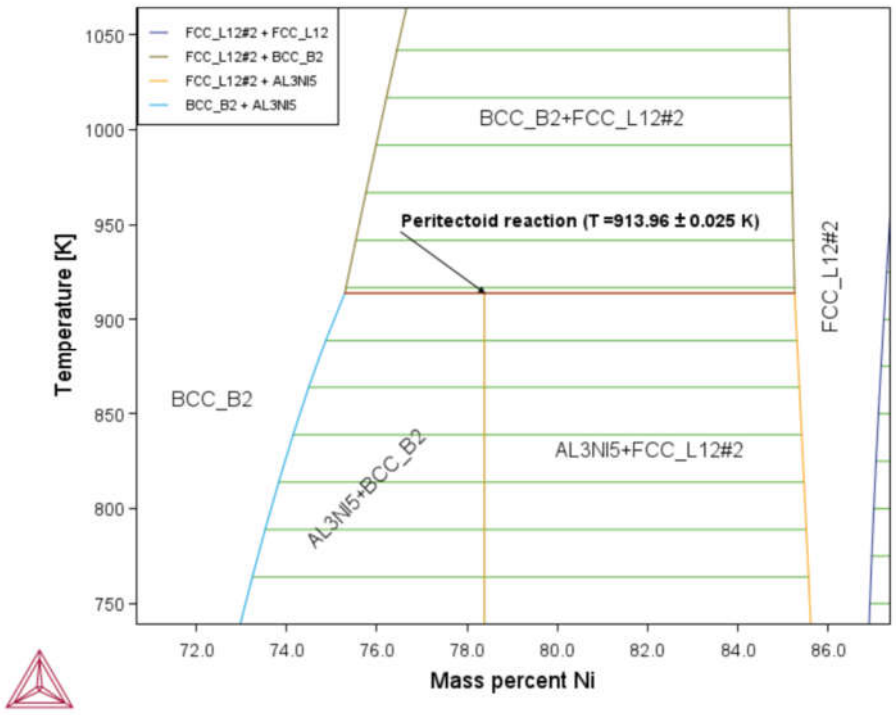

Figure 4. Enlarged portions of Figure 1 showing the peritectoid reaction for Al_3Ni_5.

By enlarging Figure 1, the solid solubility of the Ni-Al alloy binary system was determined. For the Ni-rich terminal (FCC_Ni), the maximum solid solubility of Al in Ni is 88.95 Ni mass percent at a peritectic temperature of 1642.65 K. For the Al-rich terminal (FCC_Al), the maximum solid solubility of Ni in Al is 0.51 Ni mass percent at a eutectic temperature of 914.83 K. The temperature-composition phase diagram of Figure 1 also shows the presence of three congruent melting points occurring at the elemental Al, elemental Ni, and cubic BCC_B2 (AlNi) phases with melting temperatures of 933.47 K (660.32 ^{0}C), 1728.25 K (1455.1 ^{0}C), and 1952.96 K (1679.81 ^{0}C) respectively. The first melting temperature is consistent with well-established literature melting temperature of 660 ^{0}C for aluminium [13,44]. The second congruent melting temperature is also consistent with the widely accepted melting point of 1455 ^{0}C for Ni [44–46], but 100 K higher than the value reported by [15,18]. The low melting temperature of Ni adopted could be one of the fundamental reasons why conflicting phase diagram results were obtained previously [16]. The third congruent melting temperature of the cubic BCC AlNi phase is consistent with the experimental value obtained by Refs. [26,47], but differs from the experimental values of 2600 K reported by Pasturel et al. [48] probably due to the contradictory melting temperature of Ni adopted. It is interesting to note that the Ni-Al alloy has a unique cubic BCC_B2 (AlNi) solid phase which extends from a temperature of 300 K and melts congruently at 1952.96 K without changing its phase composition extending from 60.19 to 84.20 Ni mass percent. This cubic intermetallic BCC_B2 (AlNi) phase holds a key industrial application for the Ni-Al alloy especially for high temperature related material fabrications. It has been reported that this intermetallic AlNi compound possesses ideal mechanical and thermal stability. Owing to its high melting temperature, the cubic AlNI superstructure has been found useful for protective coating [39,49], and gas-turbine applications [50].

3.2. Thermodynamic Properties

Thermodynamic properties such as Gibbs free energy, molar enthalpy, and components activity curves of the Ni-Al alloy binary system calculated relative to stable element reference (SER) is shown in Figures 5 to 7. The thermodynamic properties were investigated at three different temperatures of 915 K, 1642 K, and 1953 K. The values for the molar Gibbs energy and molar enthalpy were determined from the breadth of the curve around the minimum of the graphical plots.

Preprints (www.preprints.org) | NOT PEER-REVIEWED | Posted: 21 June 2023 doi:10.20944/preprints202306.1488.v1

Figure 5a gives the plot of the molar Gibbs free energy against Ni mass fraction for the eutectic reaction at the Al-rich terminal. Negative Gibbs energy values of -81.65 kJ/mol at 0.67 Ni mass fraction, -80.86 kJ/mol at 0.73 Ni mass fraction, and -74.60 kJ/mol at 0.42 Ni mass fraction was obtained for the Liquid, FCC_Al, and Al_3Ni phases respectively. Figure 5b shows the graphical curve of the molar Gibbs free energy against Ni mass fraction for the eutectic reaction at the Ni-rich terminal. Negative Gibbs energy values of -138.21 kJ/mol at 0.69 Ni mass fraction, -142.60 kJ/mol at 0.69 Ni mass fraction, and -134.87 kJ/mol at 0.73 Ni mass fraction was recorded for the Liquid, BCC_B2 (AlNi), and FCC_L12#2 ($AlNi_3$) phases respectively. Figure 5c shows the plot of the molar Gibbs free energy curve against Ni mass fraction for the congruent melting of the BCC_B2 (AlNi) intermediate phase to the Liquid phase. Negative Gibbs energy values of -166.29 kJ/mol, and -166.27 kJ/mol at the same 0.69 Ni mass fraction was recorded for the Liquid, and AlNi phases respectively. The negative Gibbs energy values obtained for all the phases as seen from Figures 5a – 5c is a clear indication that the Ni-Al alloy binary system is spontaneous. For the different temperatures investigates, the phase stability of the system is seen to also increase as the constant temperatures increases for Figures 5a, 5b, and 5c. This clearly suggests a strong interaction between Al and Ni in (Ni-Al) alloy with a large range of stability at 0.69 to 0.73 Ni mass fraction.

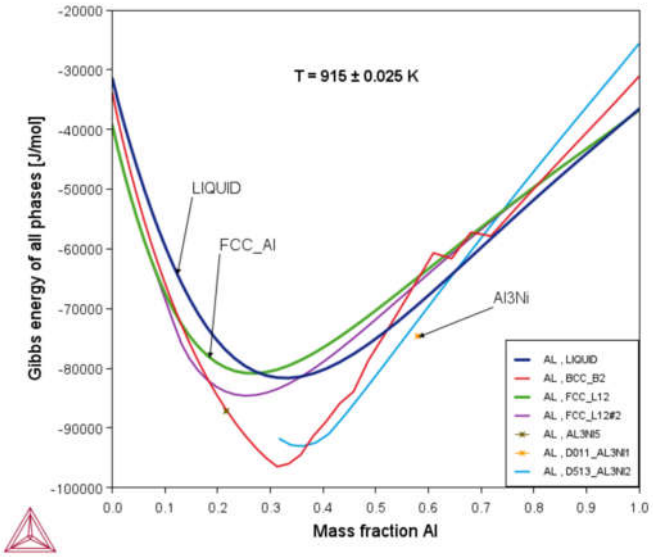

(a)

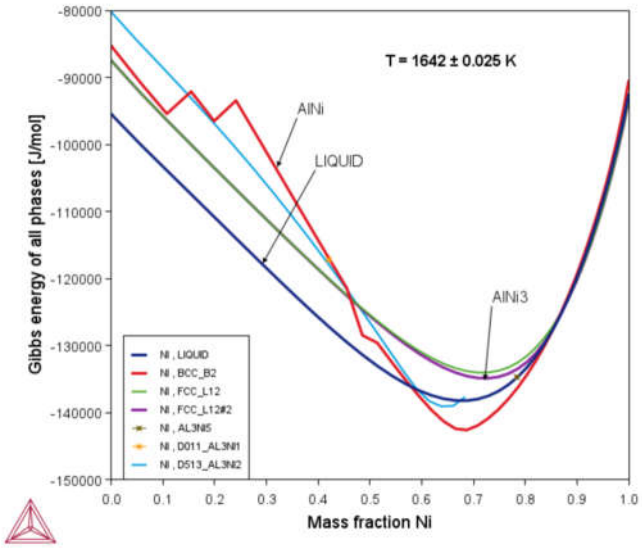

(b)

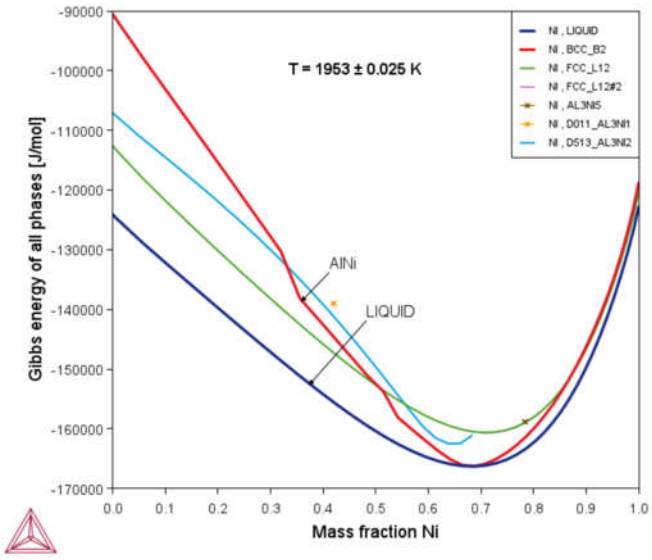

(c)

Preprints (www.preprints.org) | NOT PEER-REVIEWED | Posted: 21 June 2023 doi:10.20944/preprints202306.1488.v1

Figure 5. Gibbs free energy curve plot against Ni mass fraction for the Ni-Al alloy phases at different temperatures of (a) 915 K (b) 1642 K and (c) 1953 K.

Figures 6(a-c) shows the molar enthalpy against mass fraction Ni of all phases present in the Ni-Al alloy binary system at different temperatures of 915 K, 1642 K, and 1953 K. Figure 6a gives the result of the enthalpy of formation of the liquid phase by the Eutectic reaction at T = 915 K for the Al-rich side. Negative molar enthalpy values of -200.21 kJ/mol at 0.67 mass fraction, -237.55 kJ/mol at 0.75 mass fraction Ni, and -305.81 kJ/mol at 0.42 mass fraction Ni was obtained for the Liquid, FCC_Al, and Al_3Ni phases respectively. The negative enthalpy values obtained in Figure 6a shows that the reaction is exothermic [31]. Figure 6b equally shows the result of the molar enthalpy of formation for a eutectic reaction occurring at the Ni-rich side with T = 1642 K. Molar enthalpy values of 4.35 kJ/mol at 0.67 mass fraction Ni, −231.99 kJ/mol at 0.69 mass fraction Ni, and -6.08 kJ/mol at 0.77 mass fraction Ni was obtained for the Liquid, FCC_Al, and Al_3Ni phases respectively. Figure 6c also gives the result obtained for the molar enthalpy for the formation of AlNi phase at T = 1953 K. Molar enthalpy of 158.74 kJ/mol, and -111.09 kJ/mol at the same Ni mass fraction of 0.67 was obtained for the liquid and AlNi phases respectively. By comparing the three different temperature enthalpy plots of Figure 6, it is evident that as temperature increases, the enthalpy of the Ni-Al alloy binary system also increases with the maximum enthalpy occurring at 1953 K. This means that as more solid mixtures transcending the phases within the temperature regions under investigation continues to melt, the number of molecular interactions occurring at these different phases ultimately causes significant rise in the internal energy of the binary system. This explains why the enthalpy value for the Ni-Al binary system continues to rise until the whole solid completely melts into liquid immediately after the congruent melting temperature at 1953 K. Figure 6 clearly shows a positive increase in the enthalpy values of the LIQUID phase which rose from -200.21 kJ/mol (at 915 K), 4.35 kJ/mol (at 1642 K), up till 158.74 kJ/mol (at 1953 K).

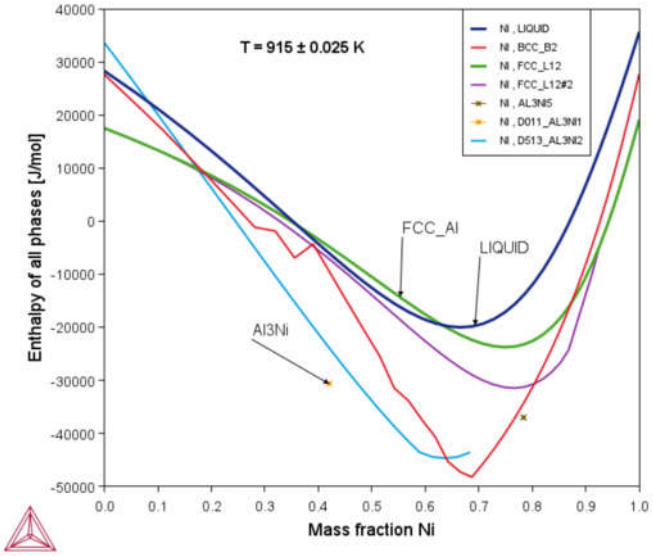

(a)

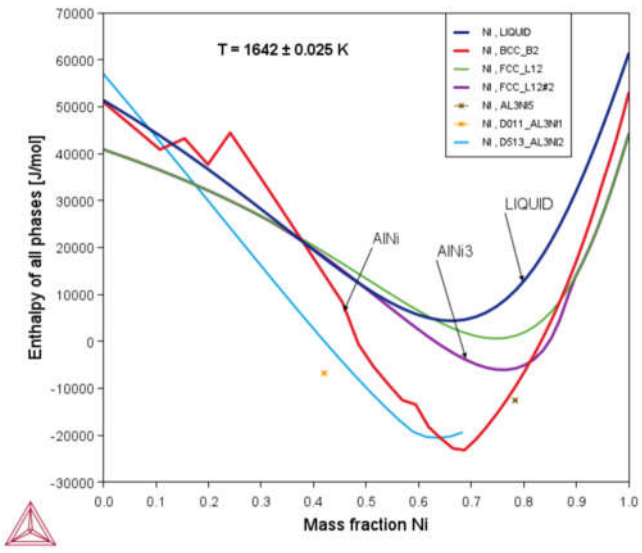

(b)

Preprints (www.preprints.org) | NOT PEER-REVIEWED | Posted: 21 June 2023 doi:10.20944/preprints202306.1488.v1

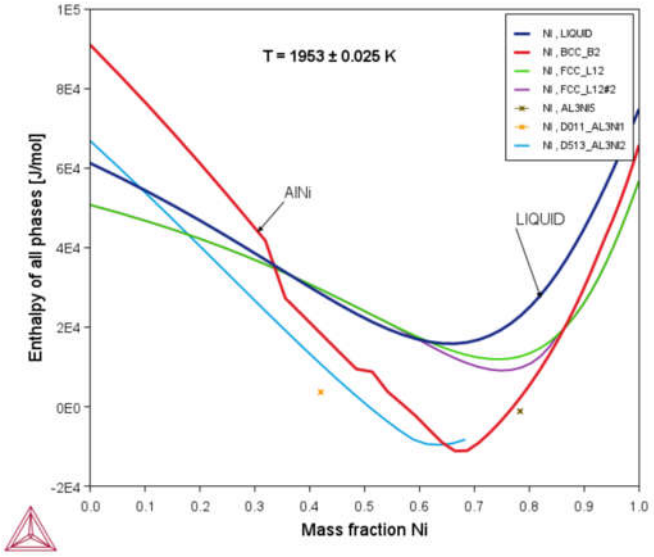

(c)

Figure 6. The plot of molar enthalpy against Ni mass fraction at different temperatures of (a) 915 K (b) 1642 K and (c) 1953 K of the Ni-Al alloy binary system.

Activities has been found to not only depend on composition but also on temperature and pressure [51]. Figures 7(a-c) shows the plot of the natural logarithm of the activity against Ni mass fraction for Ni-Al alloy at a constant pressure of 1 atm and different temperatures of 915 K, 1642 K, and 1953 K respectively. Figure 7a shows the calculated activities of Al and Ni at the Al-rich side eutectic region at T = 915 K. Figure 7b also shows the calculated activities of the intermediate AlNi and $AlNi_3$ phases in liquid for a eutectic reaction at T = 1642K. In Figure 7c, the calculated activity of the intermediate AlNi phase in liquid at T = 1953 K is shown. The result of the activities of Figure 7 shows that there is strong interaction between the atoms of the Ni-Al alloy. The Figure also shows that as the temperature increases, the activity of the alloy also increases. Another observation noted from Figures 7(a-c) is that as the activity of Ni increases, the activity of Al decreases with Ni mass fraction.

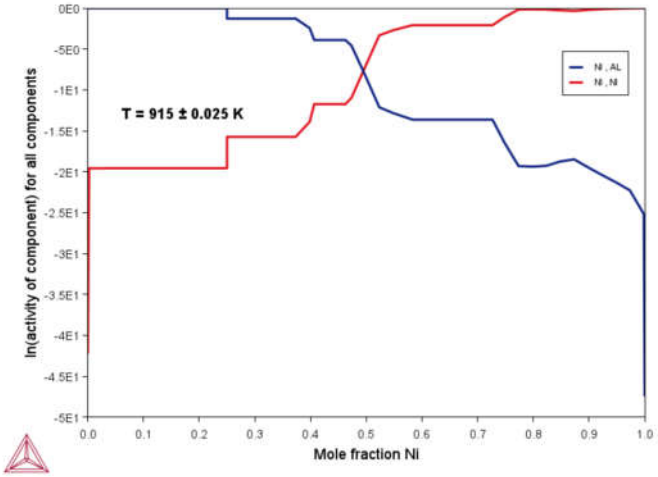

(a)

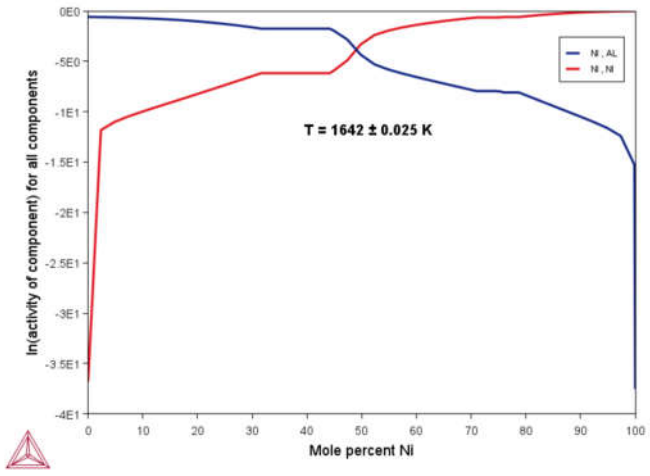

(b)

Preprints (www.preprints.org) | NOT PEER-REVIEWED | Posted: 21 June 2023 doi:10.20944/preprints202306.1488.v1

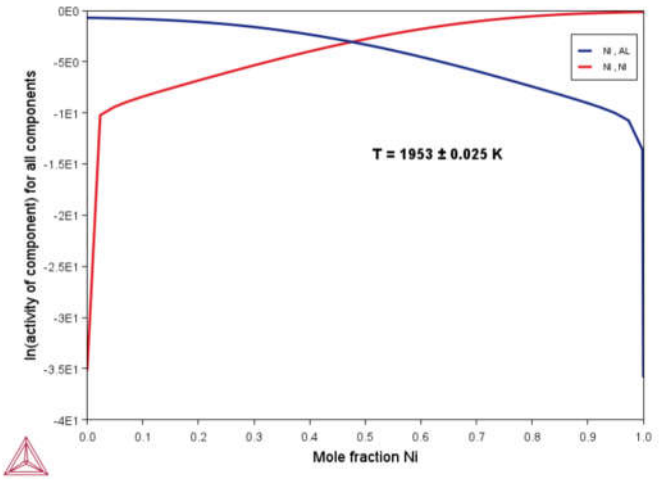

(c)

Figure 7. The natural logarithm of the activity of Ni-Al alloy binary system at different temperatures of (a) 915 K (b) 1642 K and (c) 1953 K.

4. Conclusions

The phase diagram of the Ni-Al alloy binary system has been re-assessed and the thermodynamic properties of the Ni-Al alloy determined using Thermo-Calc (TCBIN database) 2022b software. Nineteen phase fields including elemental Al and Ni was obtained from the equilibrium calculation with six singles phases fields and thirteen double phase regions obtained. The phase diagram also showed six invariant reactions with two eutectic reactions occurring at T = 914.83 K of 6.15 Ni mass percent and T = 1641.80 $\pm$ 0.025K of 86.56 Ni mass percent. Three peritectic reactions were also found at T = 1123.55 K for 42.03 Ni mass percent, T = 1400.72 K for 59.20 Ni mass percent and T = 1642.65 K for 87.30 Ni mass percent. A peritectoid reaction was equally found at T = 913.96 K for 78.38 Ni mass percent. Aside the elemental congruent melting points of Al and Ni, a third congruent melting point was observed at the BCC structure of the Ni-Al alloy at T = 1952.96 K for 86.56 Ni mass percent. The thermodynamic calculations of the binary alloy (Ni-Al) were determined at T = 915 K, 1642 K, and 1953 K with the molar Gibbs free energy cure, molar enthalpy, and the activity of the Ni-Al alloy binary system plotted against mass fraction Ni. The Ni-Al alloy binary system showed negative values for Gibbs energy indicating that the reaction at the different temperatures is spontaneous. The maximum molar enthalpy of 158.74 kJ/mol at 0.69 Ni mass fraction was obtained at T = 1953 K. With the activity value of the components less than unity, the activity plot thus showed strong interaction between the Al and Ni atoms of the alloy. The negative Gibbs value obtained is an indication the Ni-Al alloy binary system is stable and can be predicted to have good wear resistance, corrosion resistance and hardness. These results are important reference tools for further engineering metallurgy study and different industrial applications of the Ni-Al alloy binary system.

Conflict of Interest: The authors declare that they have no competing personal relationships or financial interests that could have appeared to influence the research findings presented herein.

References

[1] T. Turpin, J. Dulcy, M. Gantois, Carbon diffusion and phase transformations during gas carburizing of high-alloyed stainless steels: Experimental study and theoretical modeling, Metall. Mater. Trans. A Phys. Metall. Mater. Sci. 36 (2005) 2751–2760. https://doi.org/10.1007/s11661-005-0271-4.

[2] H.L. Chen, Q. Chen, A. Engström, Development and applications of the TCAL aluminum alloy database, Calphad Comput. Coupling Phase Diagrams Thermochem. 62 (2018) 154–171.

https://doi.org/10.1016/J.CALPHAD.2018.05.010.

[3] Thermo-Calc, The CALPHAD Methodology - Thermo-Calc Software, (2016). https://thermocalc.com/about-us/methodology/the-calphad-methodology/ (accessed August 28, 2022).

[4] S.M. Shah, N. Ullah, B. Ullah, M. Shehzad, T. Usman, Thermodynamic Analysis and Calculations of (Fe-Co) Alloy by Modeling and Simulation using Thermo-Calc Software, 1 (2018) 35–38.

[5] S.J. Ikhmayies, Thermo-Calc Determination of Phase Diagram of Si-B Binary System, Jounral Miner. Met. Mater. Soc. 73 (2020) 253–259. https://doi.org/10.1007/s11837-020-04467-z.

[6] A. J O, H. T, H. L, S. P, S. B., Thermo-Calc & DICTRA, computational tools for materials science, Calphad. 26 (2002) 273. https://doi.org/https://doi.org/10.1016/S0364-5916(02)00037-8.

[7] F. Habashi, Nickel, Physical and Chemical Properties, Encycl. Met. (2013) 1520–1520. https://doi.org/10.1007/978-1-4614-1533-6_338.

[8] Lenntech, Nickel (Ni) - Chemical properties, Health and Environmental effects, (n.d.). https://www.lenntech.com/periodic/elements/ni.htm (accessed September 28, 2022).

[9] Nickel Element Facts and Properties, (n.d.). https://www.thoughtco.com/nickel-facts-606565 (accessed September 28, 2022).

[10] Azom, Aluminium: Specifications, Properties, Classifications and Classes, (2005). https://www.azom.com/article.aspx?ArticleID=2863 (accessed August 28, 2022).

[11] Azom, Aluminium and Aluminium Alloys - Characteristic Advantages and Beneficial Properties of Aluminium Extrusions, (2008). https://www.azom.com/article.aspx?ArticleID=4192 (accessed August 28, 2022).

[12] Aluminium Alloys in the Aerospace Industry: Past, Present and Future - Jindal Aluminium Limited, (n.d.). https://jindalaluminium.com/aluminium-alloys-in-the-aerospace-industry-past-present-and-future/ (accessed September 11, 2022).

[13] V. V. Kurbatkina, Nickel Aluminides, Concise Encycl. Self-Propagating High-Temperature Synth. (2017) 212–213. https://doi.org/10.1016/B978-0-12-804173-4.00099-5.

[14] J.H. Wood and E.H. Goldman, Superalloys II, John Wiley, New York, 1987.

[15] K. Hilpert, D. Kobertz, V. Venugopal, M. Miller, H. Gerads, F.J. Bremer, H. Nickel, Phase Diagram Studies on the Al-Ni System, Zeitschrift Fur Naturforsch. - Sect. A J. Phys. Sci. 42 (1987) 1327–1332. https://doi.org/10.1515/zna-1987-1117.

[16] F.J. Bremer, M. Beyss, E. Karthaus, A. Hellwig ~, T. Schober, J.-M. Welter, H. Wenzl, EXPERIMENTAL ANALYSIS OF THE Ni-Al PHASE DIAGRAM, J. Cryst. Growth. 87 (1988) 185–192.

[17] A. Pasturel, C. Colinet, A.T. Paxton, M. van Schilfgaarde, First-principles determination of the Ni-Al phase diagram, J. Phys. Condens. Matter. 4 (1992) 945–959. https://doi.org/10.1088/0953-8984/4/4/005.

[18] J. Schramm, Pha, Z. Met. 33 (1941) 347.

[19] M. Hansen, K. Anderko, Constitution of Binary Alloys, McGraw-Hill, New York, 1958.

[20] R.P. Elliott, Constitution of Binary Alloys, First Supplement, McGraw-Hill, New York, 48AD.

[21] F.A. Shunk, Constitution of Binary Alloys, Second Supplement, McGraw-Hill, New York, 1969.

[22] W.O. Alexander, N.B. Vaughan, Phase Diagram Updates: Section HI Phase Diagram Updates AI-Ni (Aluminum-Nickel), J. Phase Equilibria. 37 (1937) 257.

[23] T.B. Massalski, Binary Alloy Phase Diagrams, Am. Soc. Met. 1 (1986) 140.

[24] P.D. Desai, Ref. Data, J. Phys. Chem. 16 (1987) 109.

[25] Y. Du, N. Clavaguera, Thermodynamic assessment of the Al-Ni system, J. Alloys Compd. 237 (1996) 20–32. https://doi.org/10.1016/0925-8388(95)02085-3.

[26] I. Ansara, N. Dupin, H.L. Lukas, B. Sundman, Thermodynamic assessment of the Al-Ni system, J. Alloys

Compd. 247 (1997) 20–30. https://doi.org/10.1016/S0925-8388(96)02652-7.

[27] L. Kaufman, H. Nesor, Coupled phase diagrams and thermochemical data for transition metal binary systems — V, Calphad. 2 (1978) 325–348. https://doi.org/10.1016/0364-5916(78)90020-2.

[28] A.K. Mallik, Computer calculations of phase diagrams, Buff. Mater. Sci. 8 (1986) 107–121.

[29] Thermodynamics Software - Thermo-Calc Software, (n.d.). https://thermocalc.com/products/thermo-calc/ (accessed September 24, 2022).

[30] Thermo-Calc Documentation Set Thermo-Calc Version 2021b, in: Introd. to Thermo-Calc, 2021: p. 341. https://www.thermocalc.com/content/uploads/Documentation/Current_Static/thermo-calc-documentation-set.pdf (accessed August 28, 2022).

[31] S.J. Ikhmayies, Phase Diagram and Thermodynamic Properties of Cu–O Binary System, Miner. Met. Mater. Ser. 4 (2021) 139–147. https://doi.org/10.1007/978-3-030-65241-8_13.

[32] R. Baur, V.GEROLD, The Existence of a Metastable Miscibility Gap in Aluminium-Silver Alloys, Acta Metall. 10 (1962) 637–645.

[33] T.H. and T.S. Kozo Osamura, Takao Nakamura, Akiko Kobayashi, Chemical composition of G.P. zones in Al-Ag Alloys, Pergamon Journals. 21 (1987) 255–258.

[34] S.S. Lim, P.L. Rossiter, J.E. Tibballs, Assessment of the AI-Ag Binary Phase Diagram, 19 (1995) 131–141.

[35] K. Osamura, T. Nakamura, A. Kobayashi, T. Hashizume, T. Sakurai, An AP-FIM study on metastable phases in Al-Ag binary alloy, Acta Metall. 34 (1986) 1563–1570. https://doi.org/10.1016/0001-6160(86)90101-X.

[36] A.J. McAlister, The Ag-AI (Silver-Aluminum) System, Bull. Alloy Phase Diagrams. 8 (1987) 526–533.

[37] T.B. Massalski, H. Okamoto, Binary alloy phase diagrams, ASM Int. (1990).

[38] A. Pasturel, C. Colinet, A.T. Paxton, M. Van Schilfgaarde, First-principles determination of the Ni-Al phase diagram, J. Phys. Condens. Matter. 4 (1992) 945–959. https://doi.org/10.1088/0953-8984/4/4/005.

[39] G.A. López, S. Sommadossi, W. Gust, E.J. Mittemeijer, P. Zieba, Phase characterization of diffusion soldered Ni/Al/Ni interconnections, Interface Sci. 10 (2002) 13–19. https://doi.org/10.1023/A:1015172710411.

[40] M. Hansen, K. Anderko, H.W. Salzberg, Constitution of binary alloys, Nature. 116 (1925) 693. https://doi.org/10.1149/1.2428700/XML.

[41] F.J. Bremer, M. Beyss, E. Karthaus, A. Hellwig, T. Schober, J.M. Welter, H. Wenzl, Experimental analysis of the Ni-Al phase diagram, J. Cryst. Growth. 87 (1988) 185–192. https://doi.org/10.1016/0022-0248(88)90163-7.

[42] J.D. Verhoeven, J.H. Lee, F.C. Laabs, L.L. Jones, The phase equilibria of N3Al evaluated by directional solidification and diffusion couple experiments, J. Phase Equilibria 1991 121. 12 (2007) 15–23. https://doi.org/10.1007/BF02663666.

[43] L. Hou, B. Li, R. Wu, L. Cui, P. Ji, R. Long, J. Zhang, X. Li, A. Dong, B. Sun, Microstructure and mechanical properties at elevated temperature of Mg-Al-Ni alloys prepared through powder metallurgy, J. Mater. Sci. Technol. 33 (2017) 947–953. https://doi.org/10.1016/J.JMST.2017.02.002.

[44] AmericanElements, Melting Point of Common Metals, Alloys and Other Materials, (2006). http://www.americanelements.com/amp.meltingpoint.html (accessed November 10, 2021).

[45] Nuclear-Power, Nickel – Melting Point – Boiling Point, (2021). https://www.nuclear-power.net/nickel-melting-point-boiling-point/ (accessed September 30, 2022).

[46] N. Institute, Key properties of nickel | Nickel Institute, (n.d.). https://nickelinstitute.org/en/about-nickel-and-its-applications/properties-of-nickel/ (accessed September 30, 2022).

[47] J.D. Cotton. R.D. Noebe and M.J. Kaufman, No Title, J. Phase Equil. 14 (1993) 579.

[48] A. Pasturel, C. Colinet, A.T. Paxton, M. Van Schilfgaarde, First-principles determination of the Ni-Al phase diagram, J. Phys. Condens. Matter. 4 (1992) 945. https://doi.org/10.1088/0953-8984/4/4/005.

[49] L. Čelko, L. Klakurková, J. Švejcar, Diffusion in Al-Ni and Al-NiCr interfaces at moderate temperatures, Defect Diffus. Forum. 297–301 (2010) 771–777. https://doi.org/10.4028/www.scientific.net/DDF.297-301.771.

[50] E. Copland, FORMATION OF γ′-Ni 3 Al VIA THE PERITECTOID REACTION: γ + β (+ Al 2 O 3) = γ′ (+ Al 2 O 3), (n.d.).

[51] D. Perkins, Activity Models, (2019). https://serc.carleton.edu/research_education/equilibria/activitymodels.html (accessed January 10, 2022).